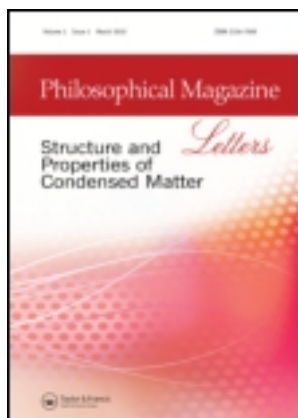


This article was downloaded by: [Pennsylvania State University]

On: 24 December 2011, At: 02:31

Publisher: Taylor & Francis

Informa Ltd Registered in England and Wales Registered Number: 1072954 Registered office: Mortimer House, 37-41 Mortimer Street, London W1T 3JH, UK



## Philosophical Magazine Letters

Publication details, including instructions for authors and subscription information:

<http://www.tandfonline.com/loi/tphl20>

### A phase-field model for deformation twinning

Tae Wook Heo<sup>a</sup>, Yi Wang<sup>a</sup>, Saswata Bhattacharya<sup>a</sup>, Xin Sun<sup>b</sup>, Shenyang Hu<sup>b</sup> & Long-Qing Chen<sup>a</sup>

<sup>a</sup> Department of Materials Science and Engineering, The Pennsylvania State University, University Park, PA 16802, USA

<sup>b</sup> Pacific Northwest National Laboratory, PO Box 999, Richland, WA 99352, USA

Available online: 07 Dec 2010

To cite this article: Tae Wook Heo, Yi Wang, Saswata Bhattacharya, Xin Sun, Shenyang Hu & Long-Qing Chen (2011): A phase-field model for deformation twinning, *Philosophical Magazine Letters*, 91:2, 110-121

To link to this article: <http://dx.doi.org/10.1080/09500839.2010.537284>

PLEASE SCROLL DOWN FOR ARTICLE

Full terms and conditions of use: <http://www.tandfonline.com/page/terms-and-conditions>

This article may be used for research, teaching, and private study purposes. Any substantial or systematic reproduction, redistribution, reselling, loan, sub-licensing, systematic supply, or distribution in any form to anyone is expressly forbidden.

The publisher does not give any warranty express or implied or make any representation that the contents will be complete or accurate or up to date. The accuracy of any instructions, formulae, and drug doses should be independently verified with primary sources. The publisher shall not be liable for any loss, actions, claims, proceedings, demand, or costs or damages whatsoever or howsoever caused arising directly or indirectly in connection with or arising out of the use of this material.

## A phase-field model for deformation twinning

Tae Wook Heo<sup>a\*</sup>, Yi Wang<sup>a</sup>, Saswata Bhattacharya<sup>a</sup>, Xin Sun<sup>b</sup>, Shenyang Hu<sup>b</sup>  
and Long-Qing Chen<sup>a</sup>

<sup>a</sup>Department of Materials Science and Engineering, The Pennsylvania State University,  
University Park, PA 16802, USA; <sup>b</sup>Pacific Northwest National Laboratory,  
PO Box 999, Richland, WA 99352, USA

(Received 25 August 2010; final version received 30 October 2010)

We propose a phase-field model for modeling microstructure evolution during deformation twinning. The order parameters are proportional to the shear strains defined in terms of twin plane orientations and twinning directions. Using a face-centered cubic Al as an example, the deformation energy as a function of shear strain is obtained using first-principle calculations. The gradient energy coefficients are fitted to the twin boundary energies along the twinning planes and to the dislocation core energies along the directions that are perpendicular to the twinning planes. The elastic strain energy of a twinned structure is included using the Khachatryan's elastic theory. We simulated the twinning process and microstructure evolution under a number of fixed deformations and predicted the twinning plane orientations and microstructures.

**Keywords:** deformation twinning; microstructure; modeling; phase-field model; first-principle calculation

### 1. Introduction

Deformation twinning is one of the two major deformation mechanisms of crystalline solids [1], the other being slipping through dislocation motion. It is widely known that deformation twinning typically takes place in materials with low-to-medium stacking fault energy and a small number of slip systems such as body-centered cubic (bcc) or hexagonal close-packed (hcp) crystals. However, deformation twinning has also been observed in many face-centered cubic (fcc) materials which have large number of slip systems and/or high stacking fault energy under severe deformation conditions such as low temperature and high strain rates [2–6], in pure [7,8], nanocrystalline materials [9–11], and at the crack tip in a polycrystal [12]. Therefore, deformation twinning is a very common phenomenon.

There have been many theoretical efforts on deformation twinning. These include phenomenological models of twin nucleation [13–16], crystallographic theoretical study on the plastic strain due to twinning [17], and first-principle calculations [18–25] and molecular dynamics (MD) simulations [8,26–29] of the atomistic

---

\*Corresponding author. Email: [tuh134@psu.edu](mailto:tuh134@psu.edu)

mechanisms of twinning, the critical shear stress for deformation twinning, and twin growth. An energetic approach to predicting the formation of twins was also proposed [30]. In addition, the factors which affect the deformation twinning behavior such as stacking fault energy, grain size, temperature [31,32], and single crystal size [33] have been discussed.

In this article, we propose a phase-field model [34–39] for predicting microstructure evolution during deformation twinning. We use fcc Al as a representative example for fcc crystals. Even though deformation twinning in Al is difficult due to its high stacking fault energy, there have been several recent reports on deformation twinning in pure Al in experiments [7–9] as well as in computer simulations such as MD simulations [8,26–29] and first-principle calculation [20]. This study describes the general framework for formulating a phase-field model for predicting microstructural evolution during deformation twinning in fcc materials using deformation energy function generated from first-principles. Thus, the formulated model is generally applicable to all fcc materials. As a first attempt, we simply employ two-dimensional (2D) simulations although the model is easily extendable to three dimensions (3D).

## 2. Model description

### 2.1. Crystallographic description

Twinning is associated with the creation of Shockley partial dislocations and twin boundaries. Thus, twinning in fcc takes place on  $\{111\}$  habit planes along  $[11\bar{2}]$  directions. Twinning process has directionality. For example, on a  $(111)$  plane, twinning along  $[11\bar{2}]$  direction is possible while it is not allowed along the  $[\bar{1}\bar{1}\bar{2}]$  direction. Such directionality can be understood with a simple crystallographic consideration or from the energy pathways for two opposite twinning modes,  $(111)[11\bar{2}]$  and  $(111)[\bar{1}\bar{1}\bar{2}]$ , obtained from first-principle calculations [23]. Therefore, the total possible number of twinning mode in fcc is 12 ( $\{111\} \langle 11\bar{2} \rangle$ ).

In Figure 1, we describe our computational cell, outlined in dashed lines in Figures 1a and b, for 2D simulation of deformation twinning on the  $(1\bar{1}0)$  plane. In this case, there are only two possible modes of twinning; one is along the  $[11\bar{2}]$  direction on the  $(111)$  habit plane (Figure 1a (variant 1)), and the other is along the  $[\bar{1}\bar{1}\bar{2}]$  direction on the  $(\bar{1}\bar{1}1)$  habit plane (Figure 1b (variant 2)). The habit planes on  $(1\bar{1}0)$  for the two modes are related by a rotation angle of  $\theta_{\text{twin}} = 70.53^\circ$  (Figure 1c). For convenience, we define new coordinate axes  $(x', y', z')$  along  $[00\bar{1}]$ ,  $[110]$ , and  $[1\bar{1}0]$  directions, respectively.

### 2.2. Phase-field formulation of deformation twinning

Within a single crystal or a given grain in a polycrystal of a fcc solid, it requires 12 order parameters,  $\eta_p (p=1, 2, 3, \dots)$ , for the 12 possible twin variants. For 2D simulations on the  $(110)$  plane, two spatially dependent fields,  $\eta_1(r)$  and  $\eta_2(r)$ , are sufficient to describe the twinning microstructures. The local twinning strains,

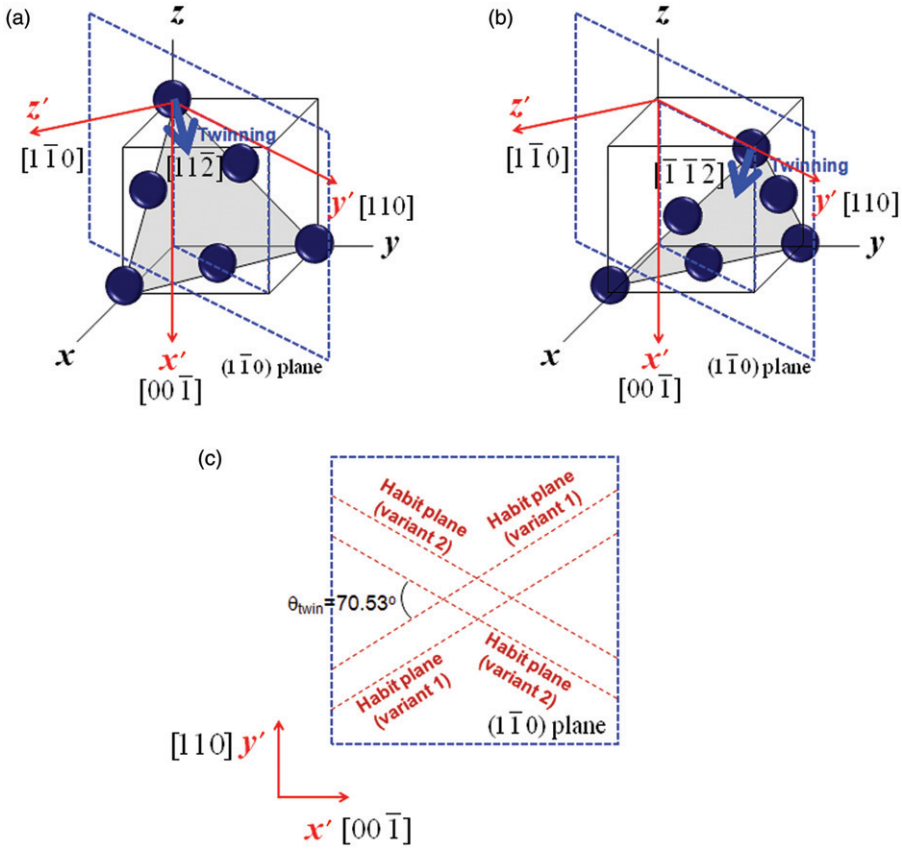


Figure 1. The crystallographic description of twinning process for (a) variant 1 and (b) variant 2. (c) The configuration of habit planes for both variants on a  $(1\bar{1}0)$  plane.

$\gamma_{(111)[11\bar{2}]}$  and  $\gamma_{(\bar{1}\bar{1}1)[\bar{1}\bar{1}\bar{2}]}$ , are related to the order parameters as

$$\begin{aligned}\gamma_{(111)[11\bar{2}]}(r) &= \eta_1(r) \cdot \gamma_{(111)[11\bar{2}]}^{\text{twin}}, \\ \gamma_{(\bar{1}\bar{1}1)[\bar{1}\bar{1}\bar{2}]}(r) &= \eta_2(r) \cdot \gamma_{(\bar{1}\bar{1}1)[\bar{1}\bar{1}\bar{2}]}^{\text{twin}},\end{aligned}\quad (1)$$

where  $\gamma_{(111)[11\bar{2}]}^{\text{twin}}$  and  $\gamma_{(\bar{1}\bar{1}1)[\bar{1}\bar{1}\bar{2}]}^{\text{twin}}$  are shear strains of fully twinned states along the  $[11\bar{2}]$  direction on the  $(111)$  plane and the  $[\bar{1}\bar{1}\bar{2}]$  direction on the  $(\bar{1}\bar{1}1)$  plane, respectively. Both of their magnitudes are equal to  $1/\sqrt{2}$  ( $=\gamma_{\text{twin}}$ ) [17,30]. Thus,  $\eta_1(r)=0$  and  $\eta_2(r)=0$  represents the original crystal,  $\eta_1(r)=1$  and  $\eta_2(r)=0$  twin variant 1, and  $\eta_1(r)=0$  and  $\eta_2(r)=1$  twin variant 2.

The deformation strain tensors of variant 1 and 2 are then given by  $\varepsilon_{ij}^{(1)} = \eta_1 \cdot \varepsilon_{ij}^{\text{twin},1}$  and  $\varepsilon_{ij}^{(2)} = \eta_2 \cdot \varepsilon_{ij}^{\text{twin},2}$ , respectively, where  $\varepsilon_{ij}^{\text{twin},1}$  and  $\varepsilon_{ij}^{\text{twin},2}$  are the twinning strain tensors associated with variants 1 and 2. To determine the twinning strain tensors for variants 1 and 2, we first defined the reference eigenstrain tensors for variant 1 ( $\varepsilon_{ij,\text{ref}}^{\text{twin},1}$ ) and variant 2 ( $\varepsilon_{ij,\text{ref}}^{\text{twin},2}$ ) which are defined in the specifically

chosen local reference frame ( $x$ -axis is defined along the twinning direction,  $y$ -axis is defined along the normal direction to habit plane, and  $z$ -axis is defined by the orthogonal to both  $x$ - and  $y$ -axis) such that it gives the pure shear strain tensors [30] as the following:

$$\left[ \varepsilon_{ij,\text{ref}}^{\text{twin},1} \right] = \begin{bmatrix} 0 & \gamma_{\text{twin}}/2 & 0 \\ \gamma_{\text{twin}}/2 & 0 & 0 \\ 0 & 0 & 0 \end{bmatrix} \text{ and } \left[ \varepsilon_{ij,\text{ref}}^{\text{twin},2} \right] = \begin{bmatrix} 0 & -\gamma_{\text{twin}}/2 & 0 \\ -\gamma_{\text{twin}}/2 & 0 & 0 \\ 0 & 0 & 0 \end{bmatrix}. \quad (2)$$

Therefore, the components of the twinning strain tensor of variant 1 ( $\varepsilon_{ij}^{\text{twin},1}$ ) in the coordinate system ( $x', y', z'$ ) are obtained by the rotation of the reference tensors as  $\varepsilon_{ij}^{\text{twin},1} = a_{im}^{R1} a_{jn}^{R1} \varepsilon_{mn,\text{ref}}^{\text{twin},1}$  and those of variant 2 are obtained by  $\varepsilon_{ij}^{\text{twin},2} = a_{im}^{R2} a_{jn}^{R2} \varepsilon_{mn,\text{ref}}^{\text{twin},2}$  where  $a_{ij}^{R1}$  and  $a_{ij}^{R2}$  are the elements of the axis transformation matrix of rotation around the  $z'$ -axis defined as

$$\left[ a_{ij}^{R1} \right] = \begin{bmatrix} \cos(-\theta_{\text{twin}}/2) & \sin(-\theta_{\text{twin}}/2) & 0 \\ -\sin(-\theta_{\text{twin}}/2) & \cos(-\theta_{\text{twin}}/2) & 0 \\ 0 & 0 & 1 \end{bmatrix} \text{ and} \quad (3)$$

$$\left[ a_{ij}^{R2} \right] = \begin{bmatrix} \cos(\theta_{\text{twin}}/2) & \sin(\theta_{\text{twin}}/2) & 0 \\ -\sin(\theta_{\text{twin}}/2) & \cos(\theta_{\text{twin}}/2) & 0 \\ 0 & 0 & 1 \end{bmatrix}.$$

In the diffuse-interface description [40], the total free energy  $F$  of the system is given by the following volume integral [41],

$$F = \int_{\Omega} \left[ f(\eta_1, \eta_2, \dots, \eta_p) + \sum_p \frac{\kappa_{p,ij}}{2} \nabla_i \eta_p \nabla_j \eta_p + \frac{1}{2} C'_{ijkl} (\varepsilon_{ij} - \varepsilon_{ij}^0) (\varepsilon_{kl} - \varepsilon_{kl}^0) \right] dV, \quad (4)$$

where  $f$  is the local deformation energy density,  $\kappa_{p,ij}$  is the gradient energy coefficient tensor in the reference frame ( $x', y', z'$ ) for the  $p$ th order parameter,  $C'_{ijkl}$  is the elastic moduli in the reference frame ( $x', y', z'$ ),  $\varepsilon_{ij}$  is the total strain tensor in the reference frame ( $x', y', z'$ ),  $\varepsilon_{ij}^0$  is the eigenstrain tensor in the reference frame ( $x', y', z'$ ), and  $\Omega$  represents the domain of interest.

### 2.2.1. Deformation energy

One of the key differences in modeling deformation twinning and structural transformations such as martensitic transformation [42,43] is the driving force. For example, the driving force for a martensitic transformation is the chemical energy difference between the parent phase and the transformed phase while in deformation twinning, the chemical free energy of a parent crystal and that of its twin state are exactly the same, i.e. there is no chemical driving force from the parent to twin state. The driving force for deformation twinning is the mechanical energy of a deformed state. The local deformation energy density  $f$  is the energy change associated with a homogeneous shear of a crystal and can be directly computed using first-principles methods [44,45]. We choose a reference state in which the lattice vectors are  $\mathbf{a}$ ,  $\mathbf{b}$ , and

$\mathbf{c}$  in the Cartesian coordinates. For programming, it is convenient to combine the three lattice vectors into a  $3 \times 3$  matrix

$$\mathbf{R} = \begin{bmatrix} \mathbf{a} \\ \mathbf{b} \\ \mathbf{c} \end{bmatrix}.$$

The homogeneous deformation of a crystal with respect to the reference state  $\mathbf{R}$  is expressed as  $\mathbf{R}' = \mathbf{R}\mathbf{X}$  where  $\mathbf{R}'$  represents the deformed state in the Cartesian coordinates and  $\mathbf{X}$  represents the deformation matrix [46]. For deformation on the (111) plane, we have

$$\mathbf{X} = \begin{bmatrix} 1 + t/2 + s/2 & t/2 & -t - s/2 \\ t/2 + s/2 & 1 + t/2 & -t - s/2 \\ t/2 + s/2 & t/2 & 1 - t - s/2 \end{bmatrix}, \quad (5)$$

where  $t$  and  $s$  represent the amount of deformation along the twinning direction  $[11\bar{2}]$  and the slipping direction  $[10\bar{1}]$ , respectively. The energies were calculated in a  $51 \times 51$  mesh in the  $t \times s$  space using the first-principles method. We employed the projector-augmented wave (PAW) method [44,45] implemented in the Vienna *ab initio* simulation package (VASP, version 4.6). The exchange-correlation functional according to Perdew–Burke–Ernzerhof (PBE) [47] was employed together with a  $20 \times 20 \times 20$   $\Gamma$ -centered  $k$ -mesh and an energy cutoff of 300 eV. We described a general deformation using the twinning and slipping directions. Thus, for pure twinning, we neglect  $s$ . The calculated deformation energy is shown in Figure 2a as a function of shear strain along the twinning direction. The variable  $t$  was converted to shear strain using the interplanar spacing of  $\{111\}$  plane. Using the relation between the shear strain and the order parameter (Equation (1)), we obtained the deformation energy as a function of order parameter along a twinning direction as shown in Figure 2b.

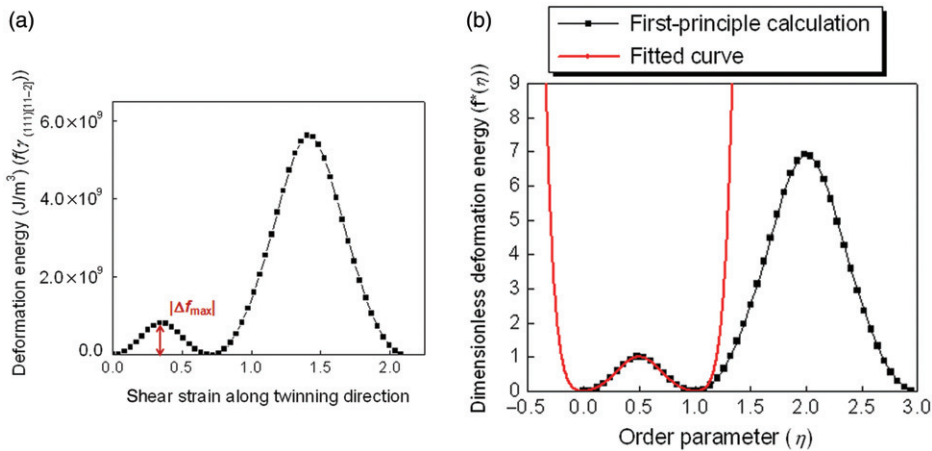


Figure 2. The deformation energy (a) calculated by the first-principle calculation and (b) its non-dimensionalized energy profile and fitted curve.

2.2.2. Gradient energy

In a twin structure, the interfacial energy between twin and original crystal is strongly anisotropic; the interfacial energy along the twin boundaries is much smaller than interfaces along other orientations. In order to take into account this anisotropy in 2D, we describe the gradient energy coefficient as

$$[\kappa_{ij}^{\text{ref}}] = \begin{bmatrix} \kappa_{11} & 0 \\ 0 & \kappa_{22} \end{bmatrix},$$

where  $\kappa_{11}$  is larger than  $\kappa_{22}$ , and the superscript ref represents reference tensor which is defined in the specifically chosen local reference frame. Thus, the gradient energy coefficients for variants 1 and 2 expressed in the coordinate system  $(x', y', z')$  are obtained by the simple rotation around the  $z'$ -axis of the reference tensor components as  $\kappa_{1,ij} = a_{im}^{R1} a_{jn}^{R1} \kappa_{mn}^{\text{ref}}$  and  $\kappa_{2,ij} = a_{im}^{R2} a_{jn}^{R2} \kappa_{mn}^{\text{ref}}$  where  $a_{ij}^{R1}$  and  $a_{ij}^{R2}$  are the elements of the rotation matrix.

2.2.3. Elastic energy

The elastic energy density represents the energy generated by the local elastic deformation in a twinned structure. The cubic elastic constants are expressed in the coordinate system  $(x', y', z')$  using the following transformation matrix:

$$[a] = \begin{bmatrix} 0 & 0 & -1 \\ 1/\sqrt{2} & 1/\sqrt{2} & 0 \\ 1/\sqrt{2} & -1/\sqrt{2} & 0 \end{bmatrix} \tag{6}$$

and  $C'_{ijkl} = a_{im} a_{jn} a_{ko} a_{lp} C_{mnop}$ . The eigenstrain  $(\varepsilon_{ij}^0)$  of the elastic energy term of Equation (4) is defined as  $\varepsilon_{ij}^0 = \sum_p \varepsilon_{ij}^{\text{twin},p} H(\eta_p)$  where  $\varepsilon_{ij}^{\text{twin},1}$  and  $\varepsilon_{ij}^{\text{twin},2}$  are the strain tensors for the twin variants 1 and 2 in the coordinate system  $(x', y', z')$ , respectively. We employed the piecewise function for  $H(\eta)$ . In order to describe the linear relation  $\eta$  and the eigenstrain, we chose  $H(\eta) = \eta$  in the range of  $\delta < \eta < 1 - \delta$  where  $\delta$  is very small value. On the other hand,  $H(\eta) = -2\eta^3 + 3\eta^2$  was chosen near the equilibrium values (0 or 1) of order parameter satisfying (i)  $H(0) = 0$ , (ii)  $H(1) = 1$ , and (iii)  $\frac{\partial H}{\partial \eta}|_{\eta=0} = \frac{\partial H}{\partial \eta}|_{\eta=1} = 0$ . Following the Khachatryan's elasticity theory [48], the total strain is separated into two contributions as  $\varepsilon_{ij} = \bar{\varepsilon}_{ij} + \delta\varepsilon_{ij}$  where  $\bar{\varepsilon}_{ij}$  is the homogeneous strain and  $\delta\varepsilon_{ij}$  is the heterogeneous strain.  $\bar{\varepsilon}_{ij}$  characterizes the macroscopic shape and volume change of the system and  $\int_{\Omega} \delta\varepsilon_{ij} dV = 0$ . To calculate the elastic strain, we solve the mechanical equilibrium equation,  $\nabla_j \sigma_{ij} = \nabla_j C'_{ijkl} (\bar{\varepsilon}_{kl} + \delta\varepsilon_{kl} - \varepsilon_{kl}^0) = 0$ , using Fourier spectral method [48]. We consider a fixed macroscopic deformation,  $\varepsilon_{ij}^a$ , i.e.  $\bar{\varepsilon}_{ij} = \varepsilon_{ij}^a$ . This is a good approximation for a grain embedded in a polycrystalline aggregate.

The evolution of order parameters are governed by the time-dependent Ginzburg–Landau (TDGL) equation [49],

$$\frac{\partial \eta_p}{\partial t} = -L \left( \frac{\delta F}{\delta \eta_p} \right) = -L \left( \frac{\partial f(\eta_p)}{\partial \eta_p} - \kappa_{p,ij} \nabla_i \nabla_j \eta_p + \frac{\partial E_{el}}{\partial \eta_p} \right), \tag{7}$$

where  $L$  is the kinetic coefficient,  $t$  is time and  $E_{el}$  is the elastic energy density. To solve the equation, we employed the semi-implicit Fourier-spectral method [50,51].

### 3. Simulation results and discussions

We chose aluminum (Al) as an example with elastic constants  $C_{11} = 114$  GPa,  $C_{12} = 62$  GPa, and  $C_{44} = 32$  GPa [24]. The twin boundary energy ( $56.5$  mJ/m<sup>2</sup> [24]) and the dislocation core energy ( $E_{core} = 4.8 \times 10^{-7}$  mJ/m [52–54]) are used to obtain the gradient energy coefficients. We approximated the interfacial energy by assuming a dislocation core at each  $\{111\}$  habit plane, i.e.  $E_{core}/d_{111} \sim 2.0$  J/m<sup>2</sup> where  $d_{111}$  is the interplanar spacing among  $\{111\}$  habit planes. All the simulations were conducted in a square domain with  $512\Delta x \times 512\Delta x$  grids where  $\Delta x$  is the grid size and was chosen as  $0.2$  nm with a periodic boundary condition. We employed dimensionless parameters in the following simulations:  $\Delta x^* = \frac{\Delta x}{l}$ ,  $t^* = L|\Delta f_{max}|t$ ,  $\kappa_{11}^* = \frac{\kappa_{11}}{l|\Delta f_{max}|}$ ,  $\kappa_{22}^* = \frac{\kappa_{22}}{l|\Delta f_{max}|}$ ,  $C_{11}^* = \frac{C_{11}}{|\Delta f_{max}|}$ ,  $C_{12}^* = \frac{C_{12}}{|\Delta f_{max}|}$ , and  $C_{44}^* = \frac{C_{44}}{|\Delta f_{max}|}$ . The characteristic length ( $l$ ) is chosen to be the same as  $\Delta x$ , and the maximum driving force ( $|\Delta f_{max}|$ ) is obtained from the deformation energy, approximately  $1.0 \times 10^9$  J/m<sup>3</sup>. The dimensionless parameters are  $\Delta x^* = 1$ ,  $\Delta t^* = 0.005$ ,  $\kappa_{11}^* = 112.0$ ,  $\kappa_{22}^* = 0.09$ ,  $C_{11}^* = 114$ ,  $C_{12}^* = 62$ , and  $C_{44}^* = 32$ .

The deformation energy ( $f$ ) was non-dimensionalized as  $f^* = \frac{f}{|\Delta f_{max}|}$  and fitted to the following polynomial  $f^*(\eta) = A_0 + A_2(\eta - 0.5)^2 + A_4(\eta - 0.5)^4 + A_6(\eta - 0.5)^6 + A_8(\eta - 0.5)^8$  as shown in Figure 2b. The values of coefficients are  $A_0 = 1.0$ ,  $A_2 = -12.43$ ,  $A_4 = 61.71$ ,  $A_6 = -152.31$ , and  $A_8 = 161.11$ . For a multi-variant system, we employ

$$f^*(\eta_1, \eta_2, \dots, \eta_p) = A'_0 + A_2 \sum_p (\eta_p - 0.5)^2 + A_4 \sum_p (\eta_p - 0.5)^4 + A_6 \sum_p (\eta_p - 0.5)^6 + A_8 \sum_p (\eta_p - 0.5)^8 + A_\gamma \sum_{p,q(\neq p)} \eta_p^2 \eta_q^2,$$

where  $A_\gamma$  is the interaction coefficient among variants.

The simulations started with a deformed state ( $\forall(\eta_1, \eta_2) = (\alpha, 0)$  or  $(0, \alpha)$ ), i.e. the system is initially under a macroscopic shear deformation. The  $\alpha$  can be any value between 0 and 1 to describe the initial deformation state. In particular, we fixed the homogeneous strain ( $\bar{\epsilon}_{ij}$ ) to  $\alpha \cdot \epsilon_{ij}^{twin,1}$  or  $\alpha \cdot \epsilon_{ij}^{twin,2}$ . Therefore, the volume average of the eigenstrain during the entire process should be equal to the fixed homogeneous strain for fixed deformation:  $\frac{1}{V} \int_{\Omega} \epsilon_{ij}^0 dV = \bar{\epsilon}_{ij}$ . To fix the deformation during the process, a penalty term [55],  $\frac{1}{2} \sum_{i,j} M_{ij} (\frac{1}{V} \int_{\Omega} \epsilon_{ij}^0 dV - \bar{\epsilon}_{ij})^2$ , is added to the free energy term, and Equation (7) becomes

$$\frac{\partial \eta_p}{\partial t} = -L \left( \frac{\partial f(\eta_p)}{\partial \eta_p} - \kappa_{p,ij} \nabla_i \nabla_j \eta_p + \frac{\partial E_{el}}{\partial \eta_p} - L \left( \sum_{ij} M_{ij} \left[ \left( \frac{1}{V} \int_{\Omega} \epsilon_{ij}^0 dV - \bar{\epsilon}_{ij} \right) \cdot \left( \epsilon_{ij}^{twin,p} \frac{1}{V} \int_{\Omega} \frac{\partial H(\eta_p)}{\partial \eta_p} dV \right) \right] \right) \right),$$

where  $M_{ij}$  are the penalty constants chosen to be  $M_{11} = 1030$ ,  $M_{12} = 3930$ ,  $M_{21} = 3930$ , and  $M_{22} = 1030$ .

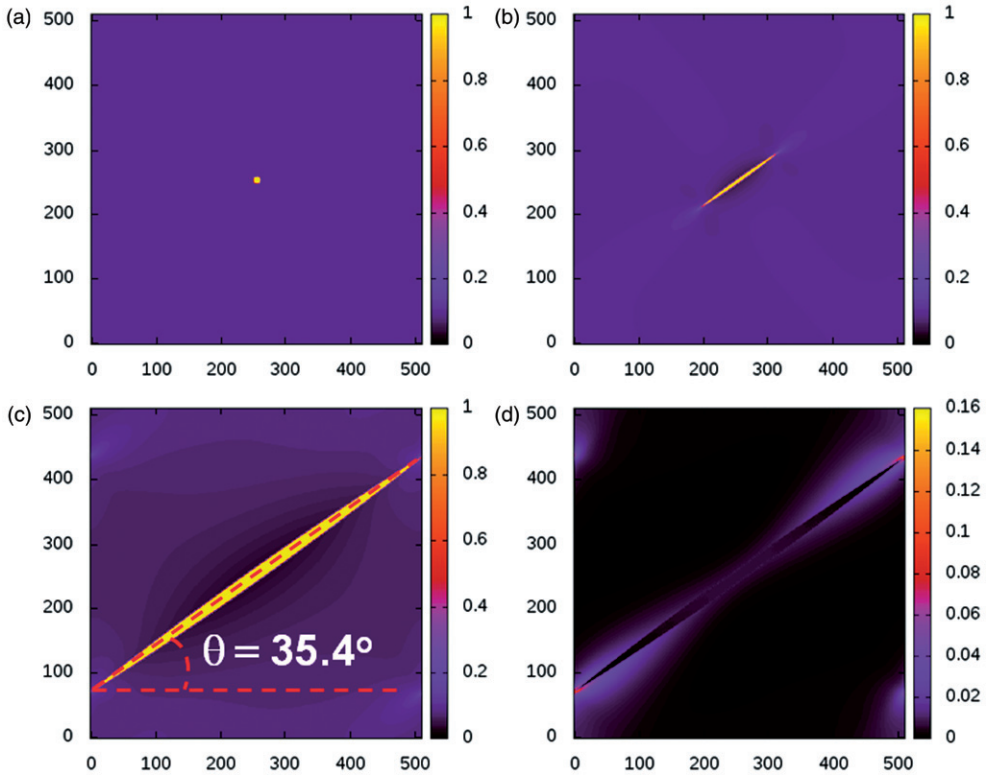


Figure 3. The growth of a single twin under a fixed macroscopic shear strain  $0.1 \cdot \varepsilon_{ij}^{\text{twin}, 1}$ . The order parameter profiles at (a) the initial state, (b)  $1000\Delta t^*$ , and (c)  $3000\Delta t^*$ . (d) The elastic energy density profile at  $3000\Delta t^*$ .

We first examined the growth aspect of a single twin under a fixed macroscopic shear strain  $0.1 \cdot \varepsilon_{ij}^{\text{twin}, 1}$ . A circular-shaped twin domain of radius  $5\Delta x$  was embedded at the center of the system as a nucleus. Figure 3 shows the temporal evolution of the growth of the single twin nucleus. Even though the initial shape of the nucleus is isotropic, the growth is strongly anisotropic, i.e. the lengthening takes place much faster than the thickening. In addition, we measured the angle between the twin lengthening direction and  $x'$ -axis, and the angle is equal to  $35.4^\circ$  as shown in Figure 3c. It agrees with a half of the dihedral angle between  $(111)$  and  $(\bar{1}\bar{1}\bar{1})$  habit planes, which means that the twin lengthens along the twin direction ( $[11\bar{2}]$ ) on the  $(111)$  habit planes and thickens along the normal direction to the habit plane. The elastic energy density profile arising from the existence of a twin also analyzed as shown in Figure 3d. The elastic energy density inside the twin and the original crystal is almost zero. Elastic energy density is only nonzero around the edge containing the array of dislocation cores. The order parameter value at this region ranges between 0 and 1 representing transition region from the undeformed original crystal ( $\eta = 0$ ) to twin ( $\eta = 1$ ). The elastic energy profile is similar to that obtained in an energy-based mechanics model in [30]. The phase-field model correctly predicts the

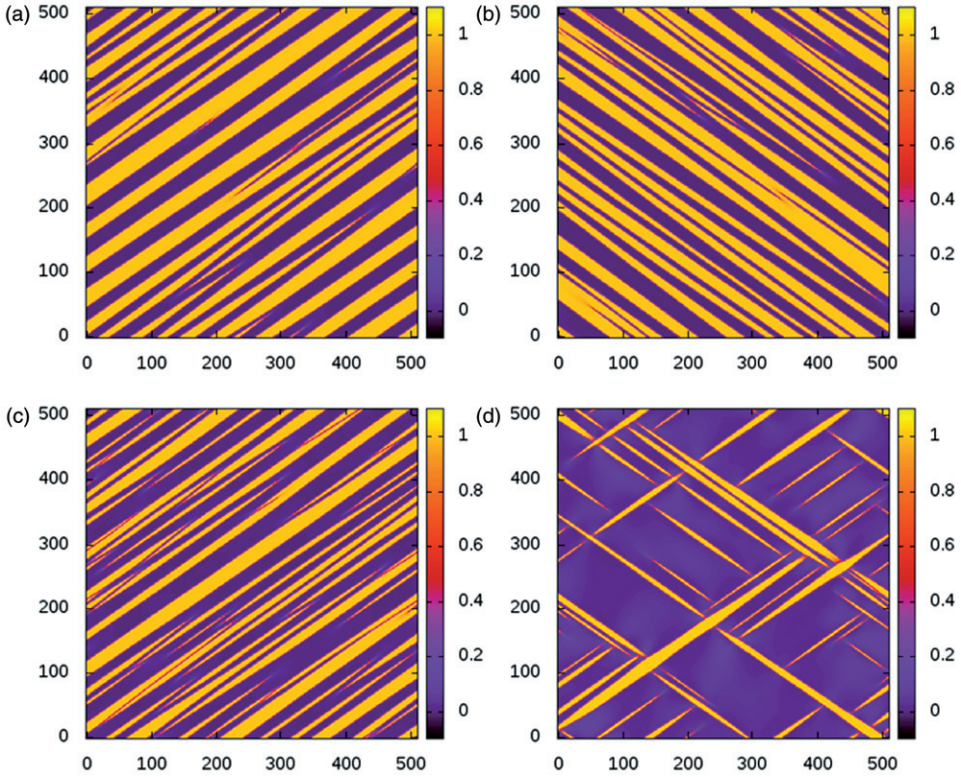


Figure 4. Twin formation when the macroscopic strain (a)  $0.5 \cdot \varepsilon_{ij}^{\text{twin},1}$ , (b)  $0.5 \cdot \varepsilon_{ij}^{\text{twin},2}$ , (c)  $0.4 \cdot \varepsilon_{ij}^{\text{twin},1}$ , and (d)  $(0.1 \cdot \varepsilon_{ij}^{\text{twin},1} + 0.1 \cdot \varepsilon_{ij}^{\text{twin},2})$  is applied. The monitor function for the case (d), we chose the  $(\eta_1 + \eta_2)$ .

crystallographically correct twin formation as a result of the interplay among the deformation energy, interfacial energy, and the elastic strain energy.

A set of simulations which involve multiple twins under several fixed macroscopic shear strains were then carried out. The initial state is a homogeneously deformed crystal with  $0.5 \cdot \varepsilon_{ij}^{\text{twin},1}$ ,  $0.5 \cdot \varepsilon_{ij}^{\text{twin},2}$ , and  $0.4 \cdot \varepsilon_{ij}^{\text{twin},1}$ , respectively, with small order parameter fluctuations to simulate severe deformation conditions. Figures 4a–c show the twin formation for the three cases, i.e. the parent crystal is under a fixed macroscopic shear strain  $0.5\gamma^{\text{twin}}$  along  $[11\bar{2}]$  direction on  $(111)$  plane,  $0.5\gamma^{\text{twin}}$  along  $[\bar{1}\bar{1}\bar{2}]$  direction on  $(\bar{1}\bar{1}1)$  plane, and  $0.4\gamma^{\text{twin}}$  along  $[11\bar{2}]$  direction on  $(111)$  plane. The homogeneously deformed crystal is transformed to a twin structure, indicating that the deformation energy in Equation (4) stored in the initial deformed crystal is dissipated by transforming into a mixture of undeformed original crystals  $((\eta_1, \eta_2) = (0, 0))$  and twins  $((\eta_1, \eta_2) = (1, 0))$ . The twin boundaries between the original crystals and twins are formed along habit planes as expected, i.e. along  $(111)$  habit planes in Figures 4a and c, and along  $(\bar{1}\bar{1}1)$  habit planes in Figure 4b. Since we consider twinning as the only deformation mode and no slipping is allowed, the equilibrium volume fraction of twin variants are expected to be related to the amount

of macroscopic deformation. We can simply expect that the larger macroscopic strain generate more twins. To verify this behavior in our model, we monitored the volume fraction of twins. We counted the number of grid points which have the order parameter greater than 0.5. The volume fraction of twin in the case where the macroscopic shear strain is  $0.4 \cdot \varepsilon_{ij}^{\text{twin},1}$  is 0.397. On the other hand, the volume fraction is 0.500 when we applied  $0.5 \cdot \varepsilon_{ij}^{\text{twin},1}$  as the macroscopic shear strain. Thus, the larger macroscopic shear strain gives rise to relatively more twins in our model.

If the macroscopic strain is relatively small, the parent crystal is metastable and twinning takes through a nucleation and growth mechanism. As an example, the initial  $\forall(\eta_1, \eta_2)$  was chosen to (0.1, 0.1). In general, the macroscopic strain in the presence of both order parameters is calculated by  $(\eta_1 \cdot \varepsilon_{ij}^{\text{twin},1} + \eta_2 \cdot \varepsilon_{ij}^{\text{twin},2})$  which is

$$\begin{bmatrix} (\eta_1 + \eta_2) \left[ -\frac{1}{2} \gamma_{\text{twin}} \sin(\theta_{\text{twin}}) \right] & (\eta_1 - \eta_2) \left[ \frac{1}{2} \gamma_{\text{twin}} \cos(\theta_{\text{twin}}) \right] & 0 \\ (\eta_1 - \eta_2) \left[ \frac{1}{2} \gamma_{\text{twin}} \cos(\theta_{\text{twin}}) \right] & (\eta_1 + \eta_2) \left[ \frac{1}{2} \gamma_{\text{twin}} \sin(\theta_{\text{twin}}) \right] & 0 \\ 0 & 0 & 0 \end{bmatrix}, \quad (8)$$

when the system deformed arbitrarily with initial order parameter  $(\eta_1, \eta_2)$ . We fixed the homogeneous strain tensor ( $\bar{\varepsilon}_{ij}$ ) to  $(0.1 \cdot \varepsilon_{ij}^{\text{twin},1} + 0.1 \cdot \varepsilon_{ij}^{\text{twin},2})$  to hold the system at a fixed macroscopically deformation. In this case, we incorporated a number of nuclei  $((\eta_1, \eta_2) = (1, 0)$  or  $(0, 1))$  into the macroscopically deformed crystals at the initial stage under the small macroscopic strain. As a nucleus, we assume the nucleus as a few stacks of planar faults with very large aspect ratio (length/thickness) [20,24,30]. We chose the layer which has the thickness  $2\Delta x$  as a nucleus. Hence, we randomly distributed the same number of the nuclei for both variants 1 and 2 for nucleation of twins in the system under the macroscopic strain. The lengthening and thickening of both variants of twins aligned along habit planes was observed under the macroscopic strain as shown in Figure 4d. In addition, the volume fraction of variants 1 and 2 are 0.085 and 0.088, respectively. It also shows the dependency of the volume fraction of twins on the amount of the macroscopic strain.

Since deformation twinning involves Shockley partial dislocations, the order parameter in the current phase-field model, related to the shear strain associated with the twinning, is similar to order parameter describing a partial dislocation [56]. However, it should be pointed out that there are significant differences between our phase-field model of deformation twinning and phase-field model of partial dislocations [56]. First of all, the dislocation model [56] employs the crystalline energy as the local free energy as a function of dislocation order parameter which is fitted to the generalized stacking fault energy ( $\gamma$ -surface calculated by the first-principle calculation) caused by the sweeping of a dislocation. On the other hand, the local free energy employed in our deformation twinning model is the deformation energy as a function of degree of crystal deformation. Deformation energy is the energy change from the original crystal state due to the homogeneous deformation of the local region participating in the twinning process. Second, the gradient energy coefficient in our model is fitted to the twin boundary energy as well as the dislocation core energy while in the dislocation model the gradient energy is only fitted to the dislocation core energy.

#### 4. Summary

A phase-field model for deformation twinning is proposed. Using aluminum as an example, the deformation energy density is obtained by means of the first-principle calculations. All the parameters such as gradient energy coefficients and eigenstrains are modeled taking into account the crystallographic information of twinning process. It is shown that the model predicts the crystallographically correct twin formation in a deformed state by taking into account twin boundary energy, the energy of the arrays of dislocation cores, and the elastic energy around the dislocation cores under the fixed macroscopic deformation condition. At large deformation, the twinning process takes place continuously as a result of absolute thermodynamic instability of the deformed state with respect to twinning. At small deformation, twinning can only take place through the nucleation and growth mechanism. In all cases, the volume fraction of twins is related to the amount of macroscopic deformation, i.e. the larger macroscopic deformation gives rise to more twins. Extension of the present model to polycrystals and to 3D is currently under way.

#### Acknowledgements

This study was supported by the Pacific Northwest National Laboratory (PNNL), the National Science Foundation (NSF) under grant number DMR0710483, and the NSF IIP-541674 through the Center for Computational Materials Design (CCMD).

#### References

- [1] J.W. Christian and S. Mahajan, *Prog. Mater. Sci.* 39 (1995) p.1.
- [2] T.H. Blewitt, R.R. Coltman and J.K. Redman, *J. Appl. Phys.* 28 (1957) p.651.
- [3] P. Haasen, *Phil. Mag.* 3 (1958) p.384.
- [4] G.T. Gray III, *Acta Metall.* 36 (1988) p.1745.
- [5] I. Karaman, H. Sehitoglu, H.J. Maier and Y.I. Chumlyakov, *Acta Mater.* 49 (2001) p.3919.
- [6] L. Bracke, L. Kestens and J. Penning, *Scripta Mater.* 61 (2009) p.220.
- [7] Q.F. Guan, Q.Y. Zhang, C. Dong and G.T. Zou, *J. Mater. Sci.* 40 (2005) p.5049.
- [8] B. Li, B.Y. Cao, K.T. Ramesh and E. Ma, *Acta Mater.* 57 (2009) p.4500.
- [9] M. Chen, E. Ma, K.J. Hemker, H. Sheng, Y. Wang and X. Cheng, *Science* 300 (2003) p.1275.
- [10] X.L. Wu, X.Z. Liao, S.G. Srinivasan, F. Zhou, E.J. Lavernia, R.Z. Valiev and Y.T. Zhu, *Phys. Rev. Lett.* 100 (2008) p.095701.
- [11] Y.T. Zhu, X.L. Wu, X.Z. Liao, J. Narayan, S.N. Mathaudhu and L.J. Kecskes, *Appl. Phys. Lett.* 95 (2009) p.031909.
- [12] B.Q. Li, M.L. Sui, B. Li, E. Ma and S.X. Mao, *Phys. Rev. Lett.* 102 (2009) p.205504.
- [13] J.B. Cohen and J. Weertman, *Acta Metall.* 11 (1963) p.996.
- [14] J.A. Venables, *J. Phys. Chem. Solids* 25 (1964) p.693.
- [15] S. Mahajan and G.Y. Chin, *Acta Metall.* 21 (1973) p.1353.
- [16] J.W. Cahn, *Acta Metall.* 25 (1977) p.1021.
- [17] B. Qin and H.K.D.H. Bhadeshia, *Mater. Sci. Tech.* 24 (2008) p.969.
- [18] S. Ogata, J. Li and S. Yip, *Science* 298 (2002) p.807.
- [19] S. Ogata, J. Li and S. Yip, *Europhys. Lett.* 68 (3) (2004) p.405.

- [20] S. Ogata, J. Li and S. Yip, Phys. Rev. B 71 (2005) p.224102.
- [21] N. Bernstein and E.B. Tadmor, Phys. Rev. B 69 (2004) p.094116.
- [22] S. Kibey, J.B. Liu, D.D. Johnson and H. Sehitoglu, Appl. Phys. Lett. 89 (2006) p.191911.
- [23] S. Kibey, J.B. Liu, D.D. Johnson and H. Sehitoglu, Appl. Phys. Lett. 91 (2007) p.181916.
- [24] S. Kibey, J.B. Liu, D.D. Johnson and H. Sehitoglu, Acta Mater. 55 (2007) p.6843.
- [25] S. Kibey, L.L. Wang, J.B. Liu, H.T. Johnson, H. Sehitoglu and D.D. Johnson, Phys. Rev. B 79 (2009) p.214202.
- [26] V. Yamakov, D. Wolf, S.R. Phillpot, A.K. Mukherjee and H. Gleiter, Nature Mater. 1 (2002) p.1.
- [27] V. Yamakov, D. Wolf, S.R. Phillpot and H. Gleiter, Acta Mater. 50 (2002) p.5005.
- [28] A. Froseth, H.V. Swygenhoven and P.M. Derlet, Acta Mater. 52 (2004) p.2259.
- [29] A. Froseth, P.M. Derlet and H.V. Swygenhoven, Adv. Eng. Mater. 7 (2005) p.16.
- [30] H. Petryk, F.D. Fischer, W. Marketz, H. Clemens and F. Appel, Metall. Mater. Trans. A 34A (2003) p.2827.
- [31] E. El-Danaf, S.R. Kalidindi and R.D. Doherty, Metall. Mater. Trans. A 30A (1999) p.1223.
- [32] M.A. Meyers, O. Vohringer and V.A. Lubarda, Acta Mater. 49 (2001) p.4025.
- [33] Q. Yu, Z.W. Shan, J. Li, X. Huang, L. Xiao, J. Sun and E. Ma, Nature 463 (2010) p.335.
- [34] L.Q. Chen, Annu. Rev. Mater. Res. 32 (2002) p.113.
- [35] W.J. Boettinger, J.A. Warren, C. Beckermann and A. Karma, Annu. Rev. Mater. Res. 32 (2002) p.163.
- [36] L. Granasy, T. Pusztai, T. Borzsonyi, G. Toth, G. Tegze, J.A. Warren and J.F. Douglas, J. Mater. Res. 21 (2006) p.309.
- [37] H. Emmerich, Adv. Phys. 57 (2008) p.1.
- [38] N. Moelans, B. Blanpain and P. Wollants, Comput. Coupling Phase Diagr. Thermochem. 32 (2008) p.268.
- [39] I. Steinbach, Modell. Simul. Mater. Sci. Eng. 17 (2009) p.073001.
- [40] J.W. Cahn and J.E. Hilliard, J. Chem. Phys. 28 (1958) p.258.
- [41] Y. Wang, H.Y. Wang, L.Q. Chen and A.G. Khachaturyan, J. Am. Ceram. Soc. 78 (1995) p.657.
- [42] Y. Wang and A.G. Khachaturyan, Acta Mater. 45 (1997) p.759.
- [43] A. Artemev, Y. Jin and A.G. Khachaturyan, Acta Mater. 49 (2001) p.1165.
- [44] P.E. Blöchl, Phys. Rev. B 50 (1994) p.17953.
- [45] G. Kresse and D. Joubert, Phys. Rev. B 59 (1999) p.1758.
- [46] Y. Wang, J.J. Wang, H. Zhang, V.R. Manga, S.L. Shang, L.Q. Chen and Z.K. Liu, J. Phys. Condens. Matter 22 (2010) p.225404.
- [47] J.P. Perdew, K. Burke and M. Ernzerhof, Phys. Rev. Lett. 77 (1996) p.3865.
- [48] A.G. Khachaturyan, *Theory of Structural Transformations in Solids*, John-Wiley and Sons, New York, 1983.
- [49] S.M. Allen and J.W. Cahn, Acta Metall. 27 (1979) p.1085.
- [50] L.Q. Chen and J. Shen, Comput. Phys. Commun. 108 (1998) p.147.
- [51] J. Zhu, L.Q. Chen, J. Shen and V. Tikare, Phys. Rev. E 60 (1999) p.3564.
- [52] M.W. Finnis and J.E. Sinclair, Phil. Mag. A 50 (1984) p.45.
- [53] M.W. Finnis and J.E. Sinclair, Phil. Mag. A 53 (1986) p.161(E).
- [54] J. Li, C.-Z. Wang, J.-P. Chang, W. Cai, V.V. Bulatov, K.-M. Ho and S. Yip, Phys. Rev. B 70 (2004) p.104113.
- [55] R. Courant, Bull. Amer. Math. Soc. 49 (1943) p.1.
- [56] C. Shen and Y. Wang, Acta Mater. 52 (2004) p.683.